Mon. Not. R. Astron. Soc. **335,** 526–538 (2002)

The symbiotic star CH Cygni – II. The ejecta from the 1998–2000 active phase

S. P. S. Eyres,[1,2★] M. F. Bode,[2] A. Skopal,[3]† M. M. Crocker,[4] R. J. Davis,[4] A. R. Taylor,[5] M. Teodorani,[6] L. Errico,[6] A. A. Vittone[6] and V. G. Elkin[7]‡

[1]*Centre for Astrophysics, University of Central Lancashire, Preston, PR1 2HE*
[2]*Astrophysics Research Institute, Liverpool John Moores University, Twelve Quays House, Egerton Wharf, Birkenhead, CH41 1LD*
[3]*Astronomical Institute, Slovak Academy of Sciences, 059 60 Tatranská Lomnica, Slovakia*
[4]*University of Manchester, Jodrell Bank Observatory, Macclesfield, Cheshire, SK11 9DL*
[5]*The Department of Physics and Astronomy, The University of Calgary, 2500 University Dr N.W., Calgary, Alberta T2N 1N4, Canada*
[6]*Osservatorio Astronomico di Capodimonte, via Moiariello 16, I–80 131 Napoli, Italy*
[7]*Special Astrophysical Observatory, Nizhnij Arkhyz 357147, Karachaevo–Cherkesia, Russia*

Accepted 2002 March 6. Received 2002 February 21; in original form 2001 June 29

ABSTRACT

We present *Hubble Space Telescope* (*HST*) imaging, a Very Large Array (VLA) radio map (4.74 GHz), optical high-resolution (echelle) spectroscopy and *UBV* photoelectric photometry of the symbiotic star CH Cyg obtained during its 1998–2000 active phase. The *HST* imaging, taken during eclipse, shows the central stars are embedded in a nebula extending to 620 ± 150 au for a distance of 270 ± 66 pc. The inner nebula is strongly influenced by the onset of activity and associated outflow in 1998. The surface brightness contours of the contemporaneous radio VLA observation agree well with *HST* images. Photometric observations of the broad 1999 *U*-minimum suggest that it is due to the eclipse of the active hot component by the giant on the long-period (14.5 yr) outer orbit. We also find that the onset of the 1998 and the 1992 active periods occur at the same orbital phase of the inner binary. Spectroscopic observations reveal two types of outflow from the active star: a high-velocity (>1200 km s^{-1}) hot star wind sporadically alternating with a more massive outflow indicated by P-Cygni-like profiles. We present evidence connecting the extended nebulosity with the high-velocity shocked outflow, and hence the activity in the central binary.

Key words: binaries: eclipsing – binaries: symbiotic – circumstellar matter – stars: individual: CH Cyg – radio continuum: stars.

1 INTRODUCTION

Symbiotic stars are an extreme case of interacting binaries, with separations of a few to a few 10s of au. They are composed of a cool component (CC), typically a red giant or Mira-type variable, and a hot component (HC), usually a white dwarf associated with an ionized component of the CC wind. An infrared sub-classification has been made, dividing the class into dusty-types (D-types), and stellar-types (S-types), based on the dominant contribution to the IR. Early modelling of the radio emission has shown that D-types typically have separations of 10 or more times that of S-types. Some of these objects show irregular optical outbursts, somewhat similar to those of dwarf novae (see e.g. Kenyon 1986; Mikołajewska 1997), (for further discussion).

CH Cyg is an S-type symbiotic star which shows such irregular outbursts or 'active phases' (see Fig. 1). It is one of the most enigmatic objects among the symbiotic stars.

Prior to 1963 it was *inactive* and often used as an MKK standard for the M6 III spectrum. Symbiotic activity was recorded for the first time at the beginning of the 1960s (Deutsch 1964). Mikkola & Tanikawa (1998) tried to explain these changes by a dynamical phenomenon known as the Kozai resonance, which causes large long-period eccentricity variations in the inner binary.

The symbiotic phenomenon of CH Cyg has no counterpart to other symbiotics in any of its main features. During active phases it develops a low excitation line spectrum and a blue continuum with a characteristic temperature of $\sim$6–9 $\times$ 10^3 K. During quiescent phases the symbiotic phenomenon practically disappears and the spectrum resembles that of an M giant.

★E-mail: spseyres@uclan.ac.uk
†Visiting Astronomer, Astrophysics Research Institute, Liverpool and Capodimonte Astronomical Observatory, Naples.
‡Visiting Astronomer, Astronomical Institute, Tatranská Lomnica.

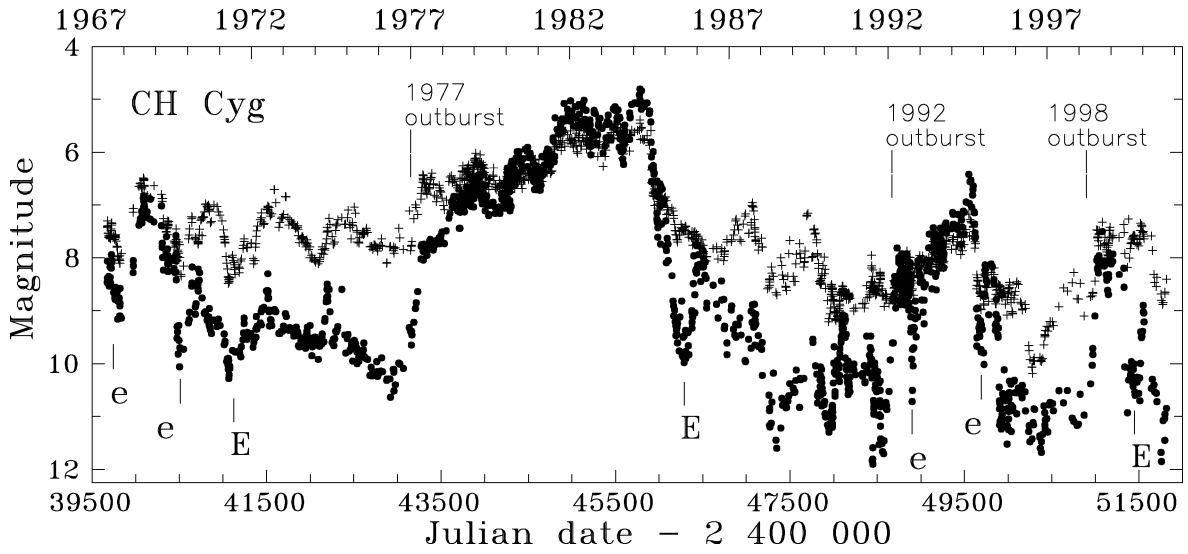

Figure 1. The $U(\bullet)$ and $V(+)$ lightcurves of CH Cyg during its symbiotic phase. Periods of activity are seen best in U. Eclipses in the outer and the inner binary are denoted by E and e, respectively.

In active phases, very complex kinematics have been observed in the circumstellar matter. At the optical maximum, in 1982–84, an irregular infall of material to the central star was indicated (e.g. Skopal, Mikołajewski & Biernikowitz 1989). The transition to quiescence, in 1984–86, was characterized by an extreme (symmetrical) expansion of the wings of hydrogen lines up to $\sim\pm2500$ km s^{-1} (Mikołajewski & Tomov 1986) and bipolar jets in the radio (Taylor, Seaquist & Mattei 1986; Crocker et al. 2001). In the 1992–95 active phase, a complex emission/absorption structure, predominately of the P-Cygni type, was a typical feature of the hydrogen line profiles (e.g. Skopal et al. 1996b).

Mikołajewski, Mikołajewska & Tomov (1987) found that CH Cyg is an eclipsing system, while Mikołajewski, Mikołajewska & Khudyakova (1990), (and references therein) found an ephemeris of $\mathrm{JD_{min}} = (2\,446\,275 \pm 75) + (5700 \pm 75) \times E$. Hinkle et al. (1993) suggested a triple-star model consisting of an inner symbiotic binary contributing the short 756-d period, in orbit with an unseen G–K dwarf on a 14.5-yr period. Skopal et al. (1996a) found that CH Cyg was an eclipsing triple, and the star on the long-period orbit is a second giant. The eclipsing nature of the system was confirmed by Iijima (1998). In this model only the symbiotic pair is responsible for the observed activity, with the HC being the active star. Preliminary fundamental parameters of the triple CH Cyg model were given by Skopal (1997). The distance to CH Cyg is 270 ± 66 pc, based on *Hipparcos* satellite measurements (Viotti et al. 1997).

Here we present contemporaneous *Hubble Space Telescope HST* and Very Large Array (VLA) imaging, high-resolution optical spectroscopy and *UBV* photometry. These were obtained during the most recent active phase of CH Cyg, which began in 1998 May.

2 OBSERVATIONS

2.1 *HST* imaging

The *HST* observations were made on 1999 August 12, as part of GO programme 8330 on symbiotic stars. Three orbits were allocated to CH Cyg, and observations were made in seven filters; F218W, F437N, F469N, F487N, F502N, F547M and F656N. These were chosen to sample a range of diagnostic lines, along with the red and UV stellar continua. The exposure times and dominant lines for images presented here are given in Table 1. Further details of these filters are available from Biretta et al. (1996). The calibrated data were retrieved from the *HST* archive. Each exposure was executed in two subexposures to allow cosmic ray subtraction. The F547M image used here was dithered to allow recovery of the full spatial resolution. The pixel size was 0.0455 arcsec for the undithered images and 0.02 275 arcsec for the dithered ones.

Table 1. *HST* observation log.

Filter	Exposure times (s)	$\bar{\lambda}$ (Å)	$\Delta\bar{\lambda}$ (Å)	Peak λ (Å)	Scientific features and wavelengths (Å)
F218W	100	2136	355.9	2091	Interstellar absorption
F437N	1000	4369	25.2	4368	[O III] λ4363
F469N	520	4695	24.9	4699	He II λ4686
F487N	200	4865	25.8	4863	Hβ λ4861
F502N	100	5012	26.8	5009	[O III] λλ4959, 5007
F547M[a]	10	5454	486.6	5362	Strömgren y
F656N	100	6562	22.0	6561	Hα λ6563

[a] Dithered image.

2.2 Optical photometry

UBV photoelectric photometry was performed using a single-channel photon-counting device mounted at the Cassegrain focus of 0.6-m reflectors at the Skalnaté Pleso and Stará Lesná observatories. HD 182691 (SAO 31623, $V = 6.525$, $B - V = -0.078$, $U - B = -0.24$) was used as a comparison star, and HD 183123 (SAO 48428, $V = 8.355$, $B - V = 0.478$, $U - B = -0.031$) as a check star. The uncertainty of these night-means is a few $\times 0.001$ mag in the V and B bands, and up to 0.02 mag in the U band.

2.3 Optical spectroscopy

High-dispersion spectroscopy was secured at the Asiago Astrophysical Observatory with the REOSC Echelle Spectrograph (RES) equipped with a CCD detector mounted at the Cassegrain focus of the 1.82-m telescope at Mt. Ekar. In 1998 the RES was equipped with a Thompson THX31156 UV-coated CCD detector with 1024×1024 19-μm pixels. Dispersions of 3.1, 3.2, 4.0 and

4.5 Å mm^{-1} were obtained in the ranges 4330–4460, 4800–4940, 5800–5990 and 6480–6670 Å respectively. Exposures of 60 min were used. The RES echelle orders were straightened using software developed at the Astronomical Observatory of Capodimonte. Thereafter the spectroscopic data were processed by using the ESO MIDAS software package in the following steps: (i) flat-field and bias subtraction, (ii) sky-background subtraction, (iii) calibration in wavelength using a thorium lamp for comparison lines, (iv) correction for heliocentric velocity and (v) normalization to the continuum level of unity.

Additional high-dispersion spectroscopy was secured at the Special Astrophysical Observatory (SAO) in Nizhnij Arkhyz. Observations on 1999 January 3 and April 5 were secured with the Main Stellar Spectrograph equipped with a CCD camera with 1040 × 1160 pixels (Panchuk 1998), located at the Nasmyth-2 focus platform of the 6-m telescope of the SAO. Spectra on 1998 September 29 and 1999 May 2 were obtained with the Coudé Echelle/Grating Spectrometer (Musaev 1998). The spectrometer, equipped with a CCD camera with 1242 × 1152 pixels, was mounted at the 1-m 'Carl–Zeiss–Jena' telescope of the SAO. Finally, the last two spectra (1999 October 2, 2000 October 15) were secured at the Terskol Observatory (3100-m altitude, northern Caucasus) with the echelle spectrometer 'Maestro', equipped with a CCD camera with 1242 × 1152 pixels, attached to the 2-m 'Carl–Zeiss–Jena' telescope.

The continuum of all the spectra was scaled to fluxes determined by contemporaneous photometric measurements. The conversion between the magnitude system and corresponding fluxes was made according to Henden & Kaitchuck (1982). The log of observations is given in Table 2.

2.4 VLA imaging

The VLA observations presented here were made on 1999 September 26 at 4.74 GHz, with a bandwidth of 50 MHz. Comparison with the primary calibrator 1331 + 305 (3C 286) gave the flux of secondary calibrator 1927 + 612 as 1.335 ± 0.009 Jy at 4.74 GHz. The complex gain solutions for this calibrator were applied to CH Cyg. The VLA observations took place 46 d after the *HST* observations, and 8 d before the last optical spectrum. Crocker et al. (2001, hereafter Paper I) gives further details of the VLA imaging since 1984.

3 RESULTS

3.1 Optical photometry

Fig. 1 shows the behaviour of the optical continuum measured photoelectrically during the symbiotic phase of CH Cyg, which started in ~1963. Variation due to activity is seen best in the *U* band. Our new observations are plotted in Fig. 2, along with the times of the optical spectroscopy, and the *HST* and VLA imaging. Each value in these figures represents the average of the observations during a night. The start of the active phase in mid-1998 is clearly seen in *B* and *U*, while the suggested eclipse ingress in mid-1999 and egress at the start of 2000 is superimposed on the decline from the active state, which ended by mid-2000. Fig. 3 shows the presence of flickering on 1998 July 30, and its absence on 1999 July 19. This flickering is seen during the active phase, but not during the postulated eclipse of the inner binary by the outer giant marked E in Fig. 1.

Table 2. Log of spectroscopic observations.

Date	Wavelength region (nm or species)	Observatory[a]
1998 Sep 5	425–680	A
1998 Sep 29	Hα, β, [O III]	SAO
1999 Jan 3	446–462	SAO
1999 Jan 5	416–689	A
1999 Apr 5	426–443 & 446–461	SAO
1999 May 2	481–488 & 655–664	SAO
1999 Oct 2	Hα, β, γ, [O III]	T
2000 Oct 15	Hα	T

[a] A – Asiago Astrophysical Observatory; SAO – Special Astrophysical Observatory; T – Terskol Observatory.

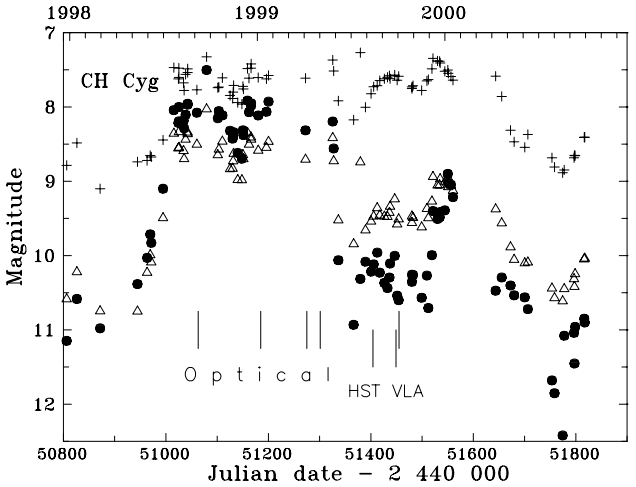

Figure 2. The $U(\bullet)$, $B(\Delta)$, $V(+)$ lightcurves of CH Cyg covering its recent (1998–2000) active phase. The minimum observed between the end of 1999 May and 2000 January was caused by the eclipse of the active star in the symbiotic pair by the giant on the outer, 14.5-yr period, orbit. The last observations made in 2000 April suggest a fading of activity. The vertical bars mark the times of our spectroscopic, *HST* and VLA observations.

3.2 *HST* WFPC2 images

The *HST* WFPC2 images from 1999 August 12 are presented in Figs 4 and 5. The central stars are located at the intersection of the diffraction spikes in e.g. Fig. 5(b). In the images dominated by the the UV continuum, [O III] lines, Hα and Hβ (Figs 4a,b,c, and 5a,b) the emission is extended at a position angle of ~165°. The extension is ~0.7 arcsec north and ~1.7 arcsec south of the central stars. The structure of the extension is most clearly defined in the F502N image (Fig. 4c), where three distinct compact components, one to the north (N) and two to the south (S1, S2) are identified. These components are also visible in the F218W image (Fig. 4a), the F437N image (Fig. 4b), the F487N image (Fig. 5a) and the F656N image (Fig. 5b). It is apparent from Fig. 5(b) that S1 and S2 are somewhat confused with the diffraction spikes due to the central stars. However, these features are visible in Fig. 4(a), where the point spread function (PSF) of the central stars is very weak. They also appear independently in each of the star-subtracted images in Figs 4 and 5. It is also possible to trace a 'loop' structure between S1 and S2, with different parts of the loop evident in different images. However the eastern edge of this loop lies along a diffraction spike, and so we cannot be confident that part is real, which is seen in Figs 4(b) and 5(a). Finally, there are partial rings of emission bracketing the central stars immediately to the east and west, the western one being most obvious in Fig. 4(a). These may again be related to the PSF of the central stars, so we cannot be certain of their reality.

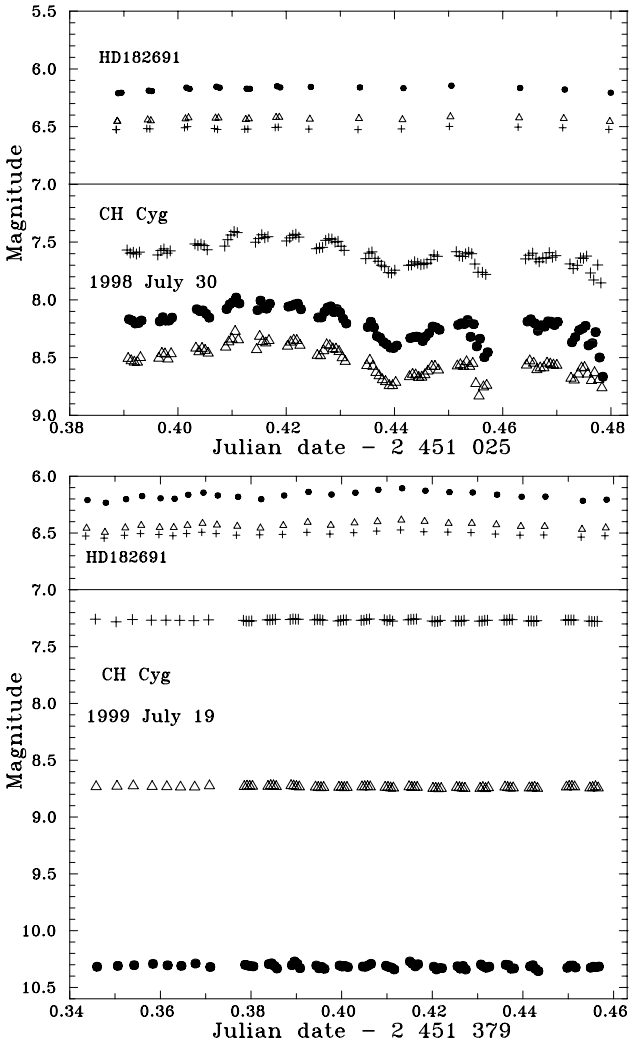

Figure 3. Example of a short-term variation during two nights located *out of* (1998 July 30) and *in* (1999 July 19) eclipse. Observations are $U(\bullet)$, $B(\Delta)$, $V(+)$ magnitudes respectively.

The ratio of the F502N map to the F437N map is very close to a map of the ratio $R_{\rm O\,III}$ of the [O III] lines around 5000 Å and the one at 4363 Å. Comparing a very approximate estimate of the continuum emission measure within the radius of the giant star with that for the extended nebula indicates that the innermost parts of the nebula have an emission measure ∼50 000 times that of the extended nebulosity. This means that the very inner regions, within the central pixel of the WFPC2 images, dominate the continuum emission, but nebular conditions result in line emission being less concentrated in the centre. Thus, we can approximately neglect continuum emission in the extended nebulosity. This analysis also explains why the λ4363-Å line is very weak or absent in the optical spectra, but is still visible in the images. Indeed, the total integrated emission in the F437N image indicates that our spectra have insufficient sensitivity to detect the extended region. The resultant $R_{\rm O\,III}$ map is presented in Fig. 4(d). In addition to features N, S1 and S2 being clearly seen in $R_{\rm O\,III}$, the loop to the south and west of the extension is picked out in high values of this ratio. Note that the region of this ratio map around the central stars cannot be used for nebular diagnostics due to the contribution from the stars and the significant continuum contribution.

3.3 Optical spectra

The spectrum from 1998 September 5 is shown in Fig. 6, and it shows the typical characteristics during the active phase. It is characterized by emission lines of low ionization potentials, including lines from O I, He I, He II, Fe II and Ti II. Similar spectra have been seen in previous active phases (e.g. Skopal et al. 1996b). TiO bands characteristic of an M giant are identifiable at λλ ∼ 4960, 5170 and 5440 Å. The detail of the development of Ti II and Fe II lines in the region λλ4495–4538 Å is shown in Fig. 7.

The [O III] 5007-Å line is also evident, and the evolution of this and nearby lines is shown in Fig. 8. We note that the [O III] 4363-Å line is absent both in and out of the postulated eclipse. The Balmer Hα, Hβ and Hγ lines are all double–peaked in this spectrum. In 1998 September these profiles are superimposed on a broad feature with a width of 1200 km s^{-1}. This feature persists in 1999, but is weaker, and disappears during the postulated eclipse of the inner binary by the outer giant (marked E in Fig. 1). The development of these lines in 1998, 1999 and 2000 is shown in Figs 9, 10 and 11, respectively. The Hα and Hβ profiles for 1999 September 5 and 1992 August 11 are compared in Figs 9(c) and 10(c), respectively, with the profiles in 1992 being single-peaked.

3.4 VLA images

The 4.74 GHz image is presented in Fig. 12(a) to facilitate comparison with the *HST* Hα and Hβ images. The southern extension is clearly seen, and the radio peak is co-incident with the central stars in the *HST* images. Notable is the fact that the extension in the radio continues significantly further to the west, and that the brightest part of the extension (the fourth contour up) is co-incident with the loop apparent in e.g. Fig. 4(c). The locations of features N, S1 and S2 are marked, allowing us to estimate the brightness temperatures at each point as $T_{\rm B,N} \sim 1600$ K, $T_{\rm B,S1} \sim 2500$ K, and $T_{\rm B,S2} \sim 260$ K, taking the size of the features in the *HST* images into account.

3.5 Nebular diagnostics

A number of diagnostics of the physical conditions in the nebula can be derived from the images presented here. The ratio $R_{\rm O\,III}$ of the F502N image (including both [O III] λλ4959 and 5007 Å) to the F437N image (including [O III] λ4363 Å) depends on both electron temperature $T_{\rm e}$ and density $n_{\rm e}$ (see Osterbrock 1989). We use the formulation presented in Eyres et al. (2001) to perform this analysis. With the caveats noted in that paper, we can draw firm qualitative conclusions from Fig. 4(d). We also note that Reiss (2000) finds that the CTE effect causes the brightness of the edge of an extended region closest to the readout amplifier to be under-estimated, but the brightness of the rest of the region to be essentially unaffected. The readout amplifier for images CH Cyg is at a position angle of 193°. This means that the calculated $R_{\rm O\,III}$ will be an under-estimate of the true value on that edge of the nebulosity.

In the case of CH Cyg, it is evident that there are strong Fe II lines in both the F437N and F502N passbands during activity (see Fig. 6). However, Fig. 11 demonstrates that Fe II is subject to eclipse, with the lines around λ4360 Å completely disappearing between 1999 April 5 and 1999 October 2. Around λ5000 Å, Fig. 8 clearly shows the Fe II line being significantly more reduced in eclipse than the adjacent [O III] line. At the time of the *HST* observations, the peak flux of the [O III] and Fe II lines are comparable, and the [O III] emission is far broader. The fact that the Fe II lines are much more strongly affected by the eclipse than the [O III] lines (and the

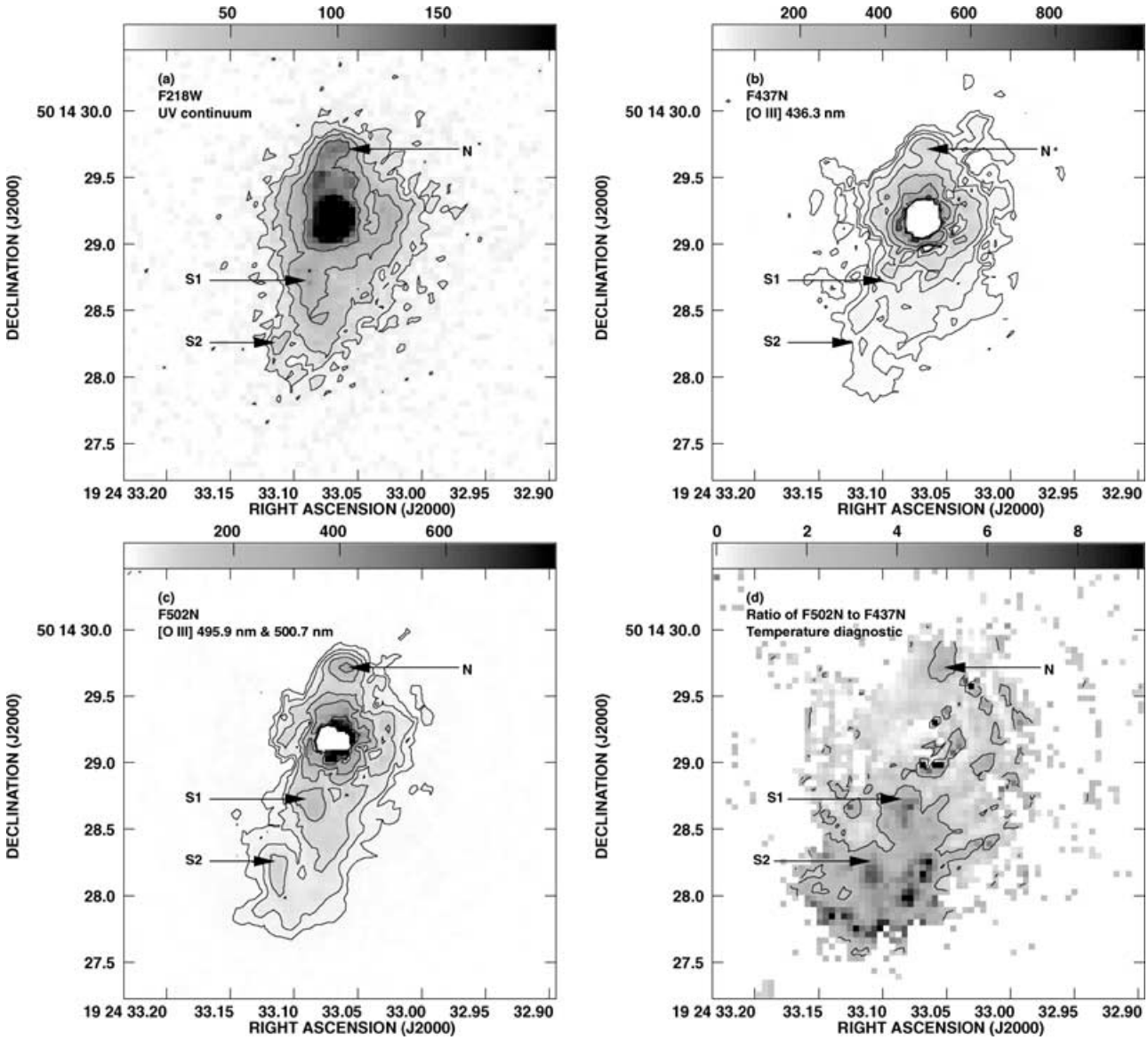

Figure 4. *HST* WFPC2 images of CH Cyg through the filters as marked. Contours are 3, 6, 12, 24, 48, 96, 192 times (a) 5×10^{-15}, (b) 3×10^{-15} and (c) 4×10^{-15} erg cm^{-2} s^{-1} Å^{-1} arcsec^{-2}. Grey-scale ranges are (a) 5×10^{-16} to 8×10^{-13}, (b) 3×10^{-15} to 1×10^{-12} and (c) 2×10^{-15} to 2×10^{-13} erg cm^{-2} s^{-1} Å^{-1} arcsec^{-2}. (b) and (c) are star-subtracted. (d) Ratio of Figs 4(b) and (c). The single contour is $R_{\rm O\,III} = 2$, grey-scale from 0 to 9.4.

complete disappearance of the Fe II lines around λ4360 Å) indicates that the Fe lines orginate close to the binary. Thus, we believe the approximate $R_{\rm O\,III}$ map is unaffected by Fe emission, except near the central stars, a region which we disregard as being unrepresentative of the nebular emission in any case.

As described by Eyres et al. (2001), radio brightness temperature $T_{\rm b}$ also depends on both electron temperature $T_{\rm e}$ and density $n_{\rm e}$. Comparing Figs 4(d) and 12(a), we can determine the conditions as a function of position. Loci for values of $R_{\rm O\,III}$, $T_{\rm b}$ and typical values of l (the path length through the nebula) are given in Figs 13(a), (b) and (c) for N, S1 and S2 respectively. It is clear that the main source of uncertainty in this analysis is the value adopted for l. A reasonable estimate would be to place it at somewhere between the largest and the smallest angular size seen on the sky. When estimated in this fashion, it also depends linearly on the distance. At a distance of 270 pc, this gives $l_{\rm N} \simeq l_{\rm S1} \simeq 70$ au, and 35 au $< l_{\rm S2} < 70$ au. It is also possible that the extended emitting region has a depth along the line of sight very much different from the extension on the sky. Thus we also rather arbitrarily consider $l_{\rm N} \simeq l_{\rm S1} \simeq l_{\rm S2} \simeq 3.5$ au and $l_{\rm N} \simeq l_{\rm S1} \simeq l_{\rm S2} \simeq 640$ au, where the former value is approximately one tenth of the smallest angular scale on the image (the width of S2) and the latter value the largest angular scale on the image (∼2.4 arcsec). We restrict this size to that region contributing to these diagrams; Corradi & Schwarz (1997) and Corradi et al. (1999) find much more extended nebulosity, but we assume we are not seeing a very extended region of radio and [O III] emission end-on. The peak values of $R_{\rm O\,III}$ are 4.5 (N), 9.5 (S1) and 7.3 (S2). From Section 3.4, we have $T_{\rm B,N} \sim 1600$ K, $T_{\rm B,S1} \sim 2500$ K, and $T_{\rm B,S2} \sim 260$ K. On inspection, it is apparent that a value of $l = 640$ au gives a locus which is nowhere near the $R_{\rm O\,III}$ locus for S2, so we do not include that locus in Fig. 13(c). Interpretation of these diagnostic diagrams is made in Section 4.5.

The F469N image (Fig. 5c) is dominated by He II λ4686 Å emission. This filter is a discriminator of strongly ionized regions (see

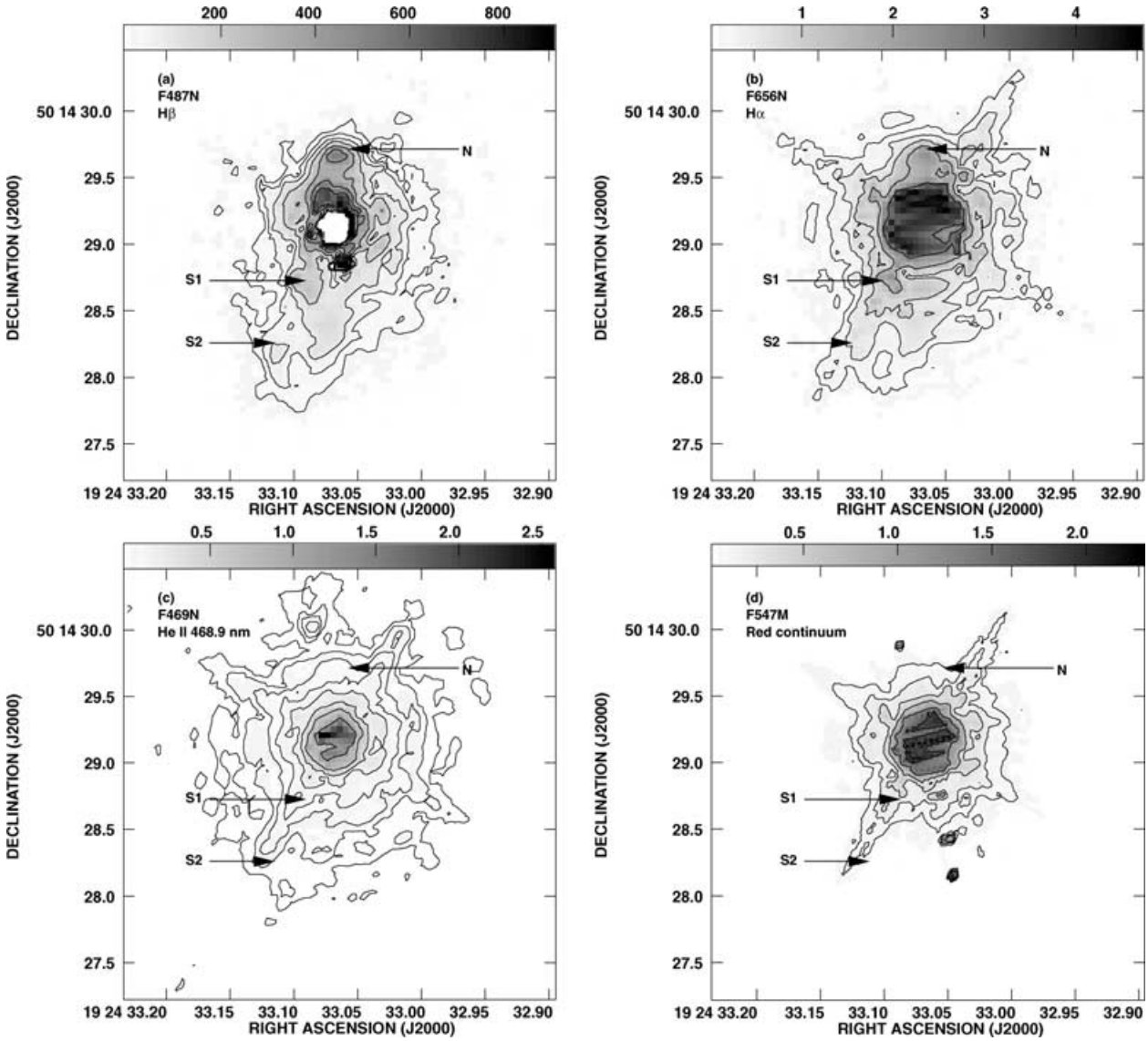

Figure 5. *HST* WFPC2 images of CH Cyg through the filters as marked. Contours are 3, 6, 12, 24, 48, and (a) 72, 96 times 6×10^{-15}, (b) 72 times 6×10^{-14} erg cm^{-2} s^{-1} Å^{-1} arcsec^{-2}, (c) 72, 96, 192 times 3×10^{-15}, (d) 72 times 2.4×10^{-14} erg cm^{-2} s^{-1} Å^{-1} arcsec^{-2}. Grey-scale ranges are (a) 6×10^{-14} to 4.7×10^{-12} and (b) 3×10^{-15} to 9×10^{-13} erg cm^{-2} s^{-1} Å^{-1} arcsec^{-2}, (c) 3×10^{-15} to 2.56×10^{-12}, (d) 2.4×10^{-14} to 2.3×10^{-12} erg cm^{-2} s^{-1} Å^{-1} arcsec^{-2}.

Osterbrock 1989). It can be seen from the image that feature N and the loop feature to the south are visible in He II.

3.6 Extinction mapping

If the radio emission is entirely thermal in nature, then the ratio of the radio emission to hydrogen line emission (e.g. Hβ) can be used to map the extinction across the nebula (Eyres et al. 2001). This in turn may be used as a tracer of nebular dust. In addition the minimum value of the extinction on this map is an upper limit on the true interstellar extinction. In the case of CH Cyg, we can compare the 4.74 GHz image (Fig. 12a) with the *HST* WFPC2 F487N image (Fig. 5a). In order that the two brightness maps could be used to form the extinction map, the radio image was divided by the beam area $\Omega = 0.1674\,\mathrm{arcsec}^2$ and the Hβ image was multiplied by the filter width $\Delta\lambda = 25.8$ Å. In addition, the Hβ image was convolved with the VLA beam to ensure the comparison of like-with-like. For $T_\mathrm{e} = 10^4$ K, the extinction is then given by

$$E(B-V) = \frac{1}{1.46} \log \frac{F_\nu}{F_\mathrm{obs}(\mathrm{H}\beta)} - 8.33 \qquad (1)$$

where $F_\mathrm{obs}(\mathrm{H}\beta)$ (erg cm^{-2} s^{-1}) is the observed Hβ flux, represented in our case by the F487N image, and F_ν (Jy) is the radio flux density, represented in our case by the VLA image. The resultant extinction map is presented in Fig. 12(b), where the image is blanked beyond where the radio flux density dropped below the 3σ limit of 0.1 mJy beam^{-1}. The range of values in the unblanked regions is $0.54 < E(B-V) < 1.6$. Note that the value of $E(B-V)$ near the central stars cannot be trusted, as the emission there is not entirely nebular. In addition, to the south-west there is radio emission where little emission is evident in the optical, leading to the high values of $E(B-V)$ seen there. For those regions where there is significant Hβ emission and little contamination from the central stars, $1 < E(B-V) < 1.2$.

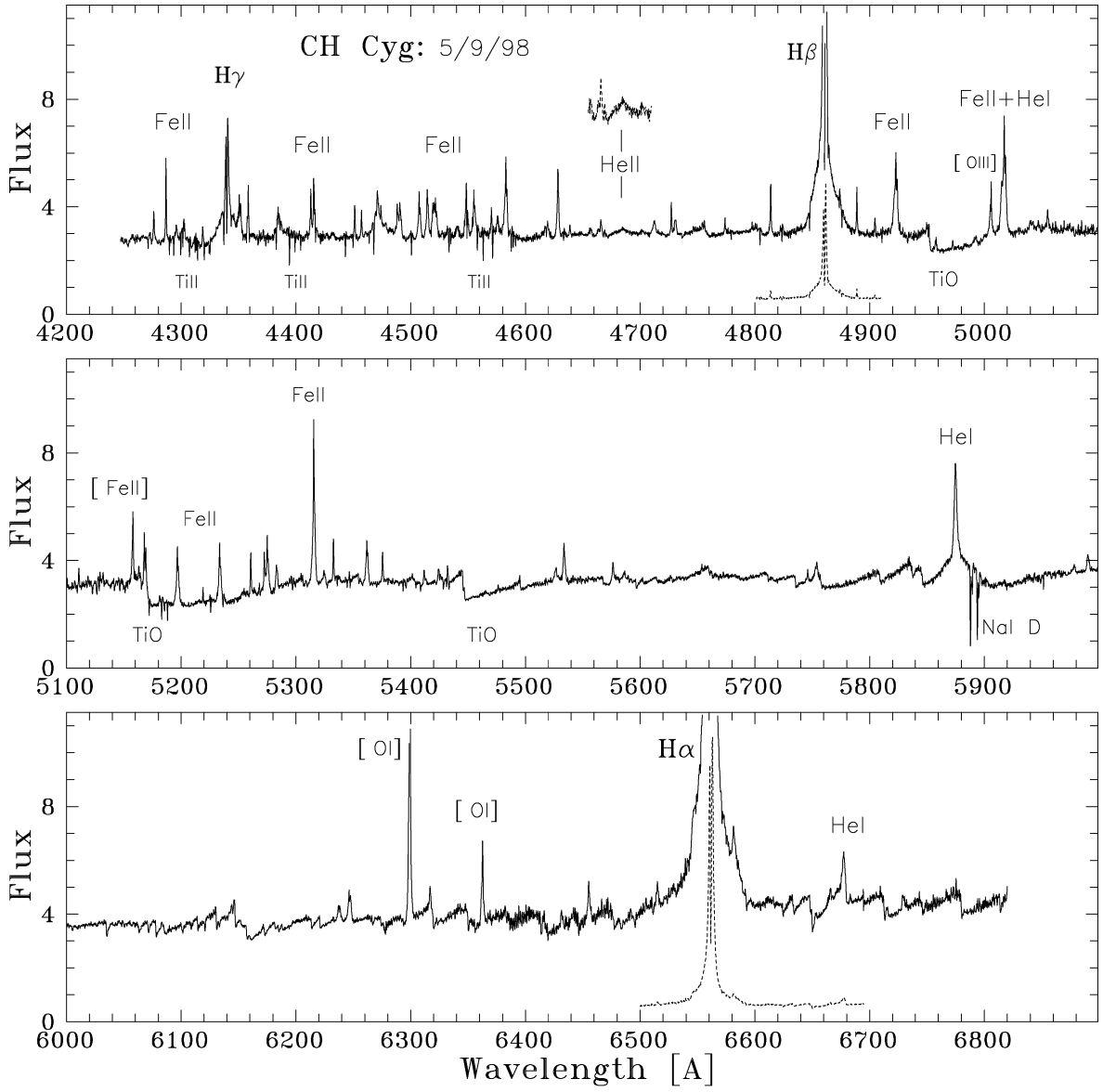

Figure 6. Spectrum of CH Cyg on 1998 September 5. The high-velocity hot star wind ($\pm$1200 km s^{-1}) developed in the H I and He I lines. Fluxes are in units of 10^{-12} erg cm^{-2} s^{-1} Å^{-1}. The He II λ4686, Hβ and Hα line profiles are also presented scaled and offset to show the detail.

4 DISCUSSION

4.1 The 1999 *U*-minimum

At the beginning of 1999 June, the brightness of the star in *U* and *B* dropped by about 2 and 1 mag, respectively, in around 10 d, and persisted at this level for ~6 months. In 1999 December we observed a sudden increase by 1 and 0.5 mag in *U* and *B*, respectively. An additional increase of brightness to ~9 in *U* was observed in 2000 January (Fig. 2). This minimum was superimposed on a decline from the peak of the active phase.

This minimum occurred close to inferior conjunction of the outer giant with the inner binary. It lasted for 6–7 months. Both the timing and the duration of the dip is similar to those of the eclipses in 1971 and 1985 (marked E in Fig. 1), and all three dips are more pronounced in *U* than in *B*. Finally, the three dips are placed around 14.5 yr apart, close to the suggested period for the outer giant from radial velocity measurements (Hinkle et al. 1993) and optical and *IUE* spectra (Mikołajeswki et al. 1990). Therefore we suggest that this minimum was caused by the *eclipse* of the active star in the symbiotic pair (i.e. the inner binary) by the giant star on the outer long-period orbit. Further observational results of ours support this interpretation as follows.

(i) The rapid (minutes to hours) variability in the blue continuum disappeared in the minimum, while out of the minimum it was seen clearly (Fig. 3). Flickering variations represent a typical feature of CH Cyg activity. Such variability is generally thought to be connected with variations in mass-transfer rates, and hence active regions of an accretion disc. Flickering has already been reported by many authors (e.g. Slovak & Africano 1978), but its absence during eclipse is a new result.

(ii) Fluxes in the hydrogen Balmer lines faded significantly (Hγ line disappeared) on 1999 October 2 (Figs 9, 10 and 11). Again, if the Balmer lines are associated with either an accretion disc or a mass outflow in the inner binary, this would support the eclipse

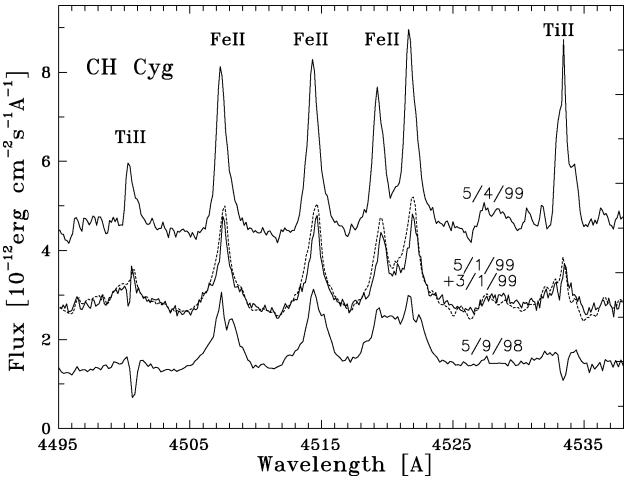

Figure 7. Detail of the devlopment of Ti II and Fe II lines between 1998 September 5 and 1999 April 5.

hypothesis. However, Figs 5(a) and (b) show that there is an extended component to the wavelength regions around the Hβ and Hα lines. There is an insignificant continuum contribution to the extended nebulosity (see Section 3.2 above). In addition, neither of these lines disappear completely during the *U* minimum.

(iii) The nebular [O III] 5007-Å line was, however, still present on 1999 October 2, and its flux was less than, but comparable with, that observed out of the eclipse, while the He I 5016-Å line faded significantly with respect to 1998 September 5 (cf. Fig. 8). From Fig. 4(c), a significant part of the [O III] line flux may originate from the extended nebula, and hence would not be eclipsed by the outer giant.

The fact that we could not differentiate the peaks in the F218W (ultraviolet continuum) and F547M (red continuum) filters is consistent with the stars being in or close to eclipse during our observations.

4.2 The line profiles

Hydrogen Balmer lines dominate the optical line spectrum of CH Cyg during its active phases. The line profiles display significant variations (Figs 9, 10 and 11). On 1998 September 5 we observed double-peaked profiles, symmetric with respect to the central absorption, superposed on a broad emission extended to about $\pm$1200 km s^{-1}. On September 29 the profiles were still of the same type, but the broad wings were less pronounced. This basic double-peaked morphology of the hydrogen profiles was also observed during the main 1977–85 activity (Hack et al. 1988; Anderson, Oliversen & Nordsieck 1980). The very broad emission suggests the presence of a high velocity hot star wind, while the double-peaked central part of the profile is consistent both with an accretion disc around the hot star or an expanding shell. The accretion disc interpretation is in agreement with previous works of Robinson et al. (1994) and Skopal et al. (1998a). In addition, an accretion disc located at the orbital plane would divide the source of radiatively driven particles into two parts, which would naturally lead to the bipolar nature of the nebula (Figs 4, 5 and 12, and Paper I). However our data cannot clearly distinguish between an accretion disc and an expanding shell of material

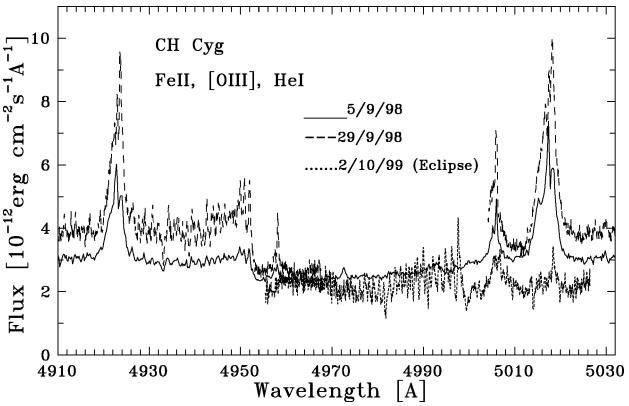

Figure 8. Development of the nebular [O III] 5007-Å line is connected with the extended nebula surrounding CH Cyg. The line is seen well also during eclipse. Note that the He I 5016 -Å line is subject to eclipse.

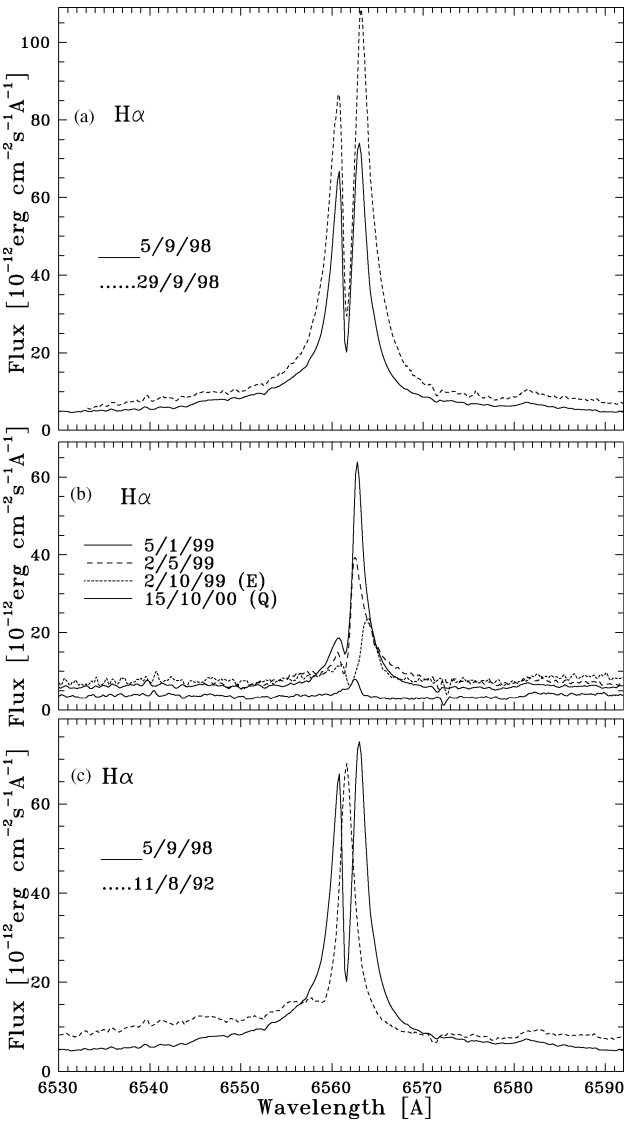

Figure 9. Evolution in the Hα line on our spectrograms. (a) Symmetrical double-peaked profiles in 1998 with broad wings extended to about $\pm$1200 km s^{-1}. (b) The profiles in 1999 are significantly influenced by a strong blueshifted absorption, and by 2000 the Hα emission is significantly reduced. (c) Comparison of typical profile observed during 1992–95 activity with that from the current outburst.

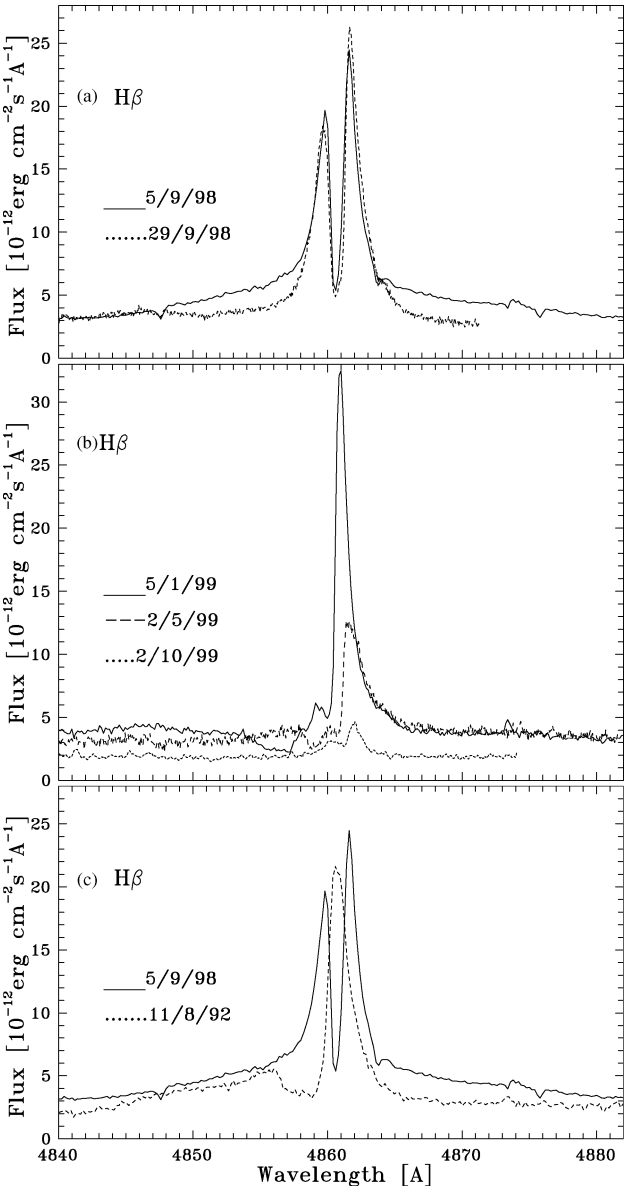

Figure 10. As in Fig. 9, but for Hβ.

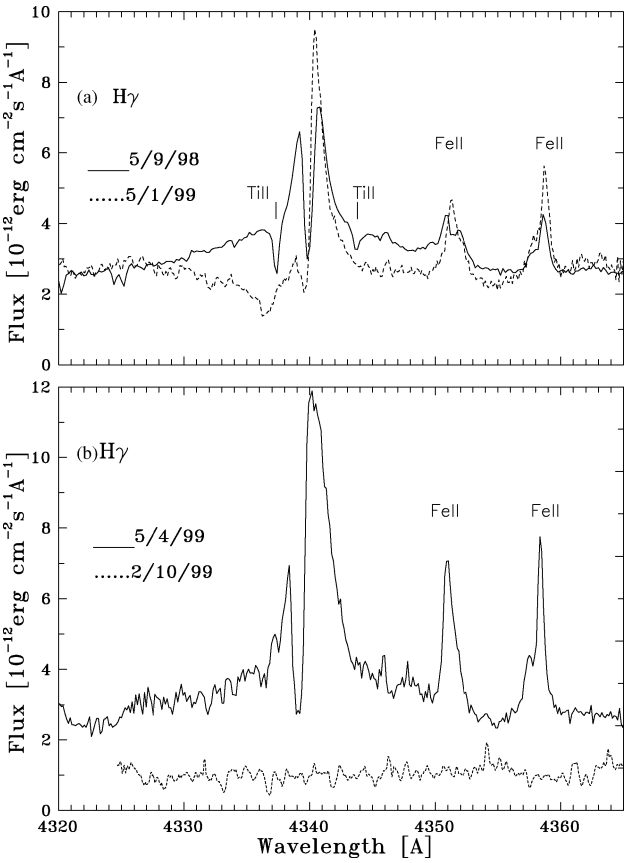

Figure 11. As in Fig. 9, but for Hγ. No 1992 comparison spectrum is available. During the eclipse the Hγ emission disappeared.

On 1999 January 5 the double-peaked profiles were significantly influenced by a strong blueshifted absorption component. As a result an absorption/emission structure had developed on the blue side of the lines – best seen in Hβ and Hγ (Figs 10 and 11), superimposed on the double-peaked structure. This dramatic development was similar to that observed during the previous 1992–95 active phase (Skopal et al. 1996b). Such evolution is consistent with an irregular mass outflow from the central star, probably more massive than via the hot wind. On 1999 April 5 the basic structure of the Hγ line profile returned to that observed on 1998 September 5 (however, only the region with Hγ was secured; compare Figs 11a and b), and on 1999 May 2 the profile was similar again to that of 1999 January 5. Finally, on 1999 October 2 emission in the hydrogen lines significantly decreased, with Hγ disappearing entirely, and the profiles lost the main characteristics observed on previous spectra. This occurred during the eclipse of the inner binary by the outer giant. The spectrum of 2000 October 15 (Fig. 9b) during the post-activity quiescent state, shows the emission in the Hα has significantly decreased. Only a faint emission placed at ~6562 Å can be seen. No signs of the mass outflow are present. This supports the connection of strong Hα emission with activity in CH Cyg, as suggested by Bode et al. (1991). We note that CH Cyg has shown evidence of both outflow (e.g. this paper) and infall (e.g. Skopal et al. 1989) during active phases.

The most interesting result is the presence of two types of mass outflow from the active star – indicated unambiguously by our observations for the first time. These are an optically thin outflow, causing the broad >1200 km s^{-1} feature, and an irregular optically thick outflow, suggested by the blueshifted absorption of the double-peaked hydrogen lines. The development of a high velocity stellar wind must be connected with the luminosity increase of the central active object. An ignition of the central parts of the accretion disc possibly results from a sudden increase of the transferred material from the giant star. This view is supported by the fact that both the 1992 and the 1998 outbursts began at the same orbital phase of the symbiotic pair, about 0.15 P_{orb} prior to periastron passage (Fig. 14). An increase of the blue continuum around the position of periastron was already noted by Skopal et al. (1996b), (see their Fig. 2). This type of mass outflow was *not* clearly seen during the 1992–95 activity, but dominated during the 1984–86 transition from activity. We note that the rise in activity in 1977 occurred around apastron passage, but that activity phase was more prolonged than the two subsequent ones starting in 1992 and 1998.

In Fig. 7, we see that on 1998 September 5 the Ti II lines were dominated by a central absorption feature, which also weakly modifies the Fe II emission profiles. Emission wings of these lines were

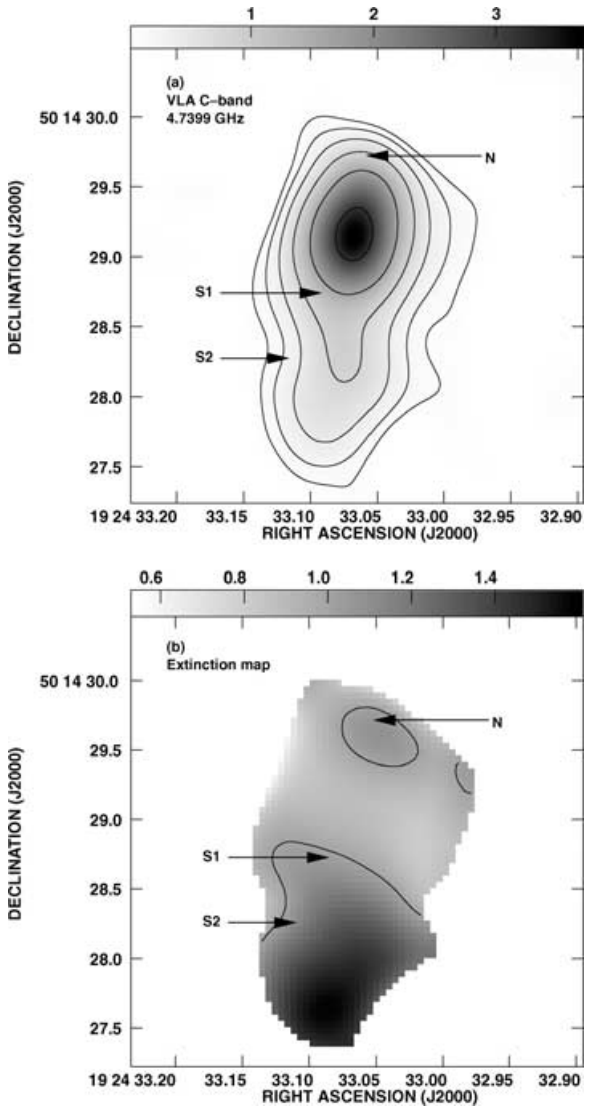

Figure 12. (a) VLA image at 5 GHz. Contours are 3.3×10^{-5} times -3, 3, 6, 12, 24, 48, 96; grey-scale is 3.3×10^{-5} to 3.7×10^{-3} Jy beam^{-1}. (b) Extinction map derived from Figs 5(a) and 12(a). The single contour is $E(B-V) = 1$; grey-scale range 0.54 to 1.6. (See Section 4.3 for caveats on interpretation of the deduced extinction values.)

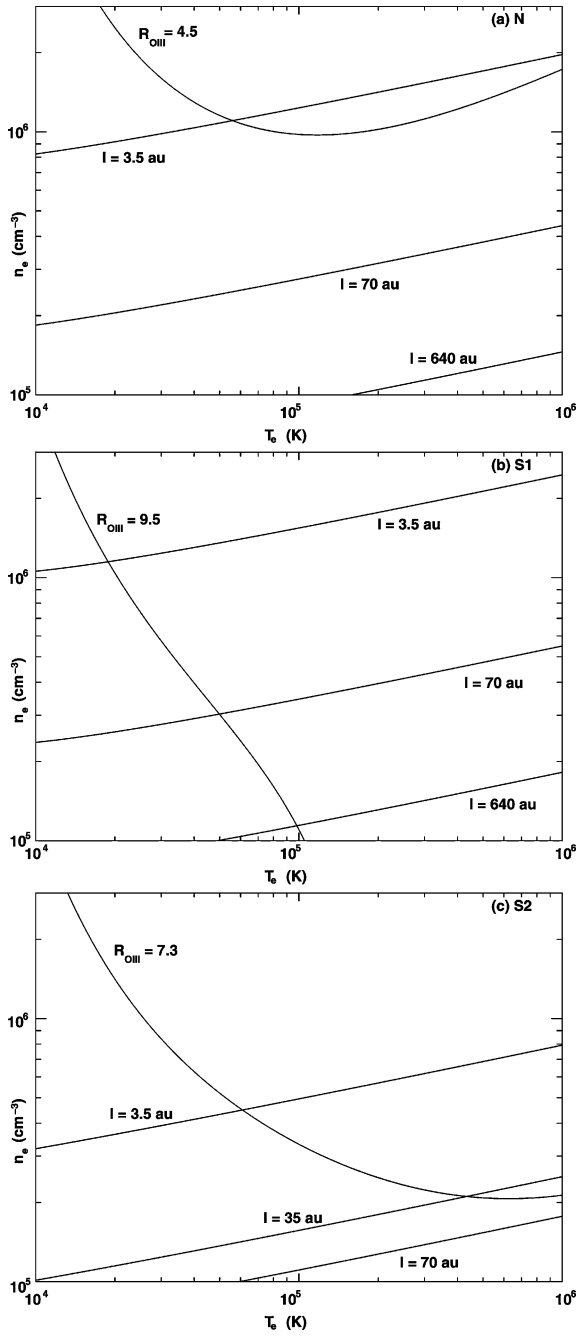

Figure 13. Diagonstic diagrams for (a) feature N, $T_b = 1600$ K, (b) feature S1, $T_b = 2500$ K, (c) feature S2, $T_b = 260$ K. Values of ratio $R_{O\,III}$ and path length l are as marked.

extended to about ± 200 km s^{-1}. By 1999 January the emission is narrower (± 150 km s^{-1}), and the absorption fainter and shifted blueward. Our last spectrum on 1999 April 5 shows only emission components of both the Ti II and the Fe II lines are present. The profiles extend to about ± 50–100 km s^{-1}. An absorption feature probably cuts the Ti II emission profile from its blue side. Qualitatively, such evolution corresponds to expansion of a shell, which gradually becomes optically thinner. However, evolution in the hydrogen lines indicates that the process of such expansion is very complex, resulting in the high-velocity mass outflow from the active star in CH Cyg.

A massive outflow which totally destroys the blue wing of the emission profile resembles that observed in other symbiotics during outburst stages (e.g. BF Cyg – Cassatella et al. 1992; Skopal et al. 1997). At present, the physical nature of such activity is rather uncertain. According to energy balance, it was suggested that the outburst of BF Cyg is powered by a thermonuclear runaway (Cassatella et al. 1992), however there are problems explaining the short recurrence time between outbursts (cf. Sion 1997). In the case of CH Cyg, both the very low luminosity and short recurrence time (cf. Fig. 1) are in conflict with such an explanation. Therefore, the question 'What powers the high-velocity mass outflow from the central star?' remains open.

It is also of interest to compare hydrogen profiles observed during the 1992–95 active phase with those measured during the present activity (bottom panel of Figs 9 and 10). The location of the main emission component of the line profiles from 1992–95 coincides with the central absorption being presented during the 1998–2000

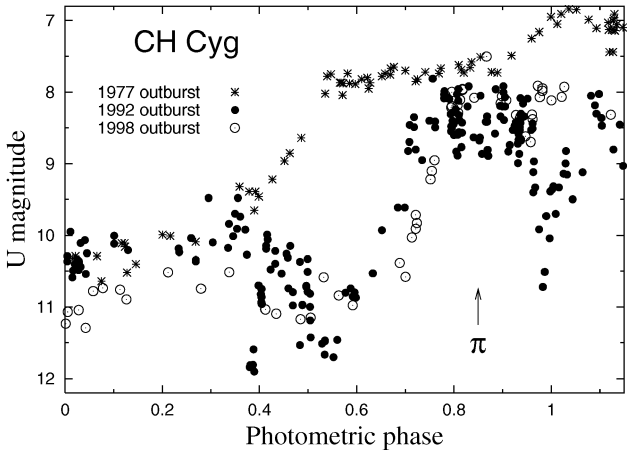

Figure 14. The onset of active phases as a function of the orbital phase of the inner binary (756-d period). Both the 1992–95 and the 1998–2000 outbursts of CH Cyg started at the same orbital phase (within the uncertainties in JD_0 and $P_{\rm orb}$), $\sim 0.15 P_{\rm orb}$ prior to the periastron passage (marked π). Orbital phase was calculated as in Skopal (1995).

outburst. Qualitatively, it indicates that the accreted material around the active star was more massive during the recent activity.

4.3 The extinction towards CH Cyg

Many previous estimates of $E(B-V)$ exist, and are given in Table 3. It is clear that fitting the 2200 Å interstellar feature and photometric studies of the field around CH Cyg (Mürset et al. 1991; Selvelli & Hack 1985; Slovak 1982; Slovak & Africano 1978) give low values $[0.01 < E(B-V) < 0.1]$ while assuming emission from thermal gas at 10^4 K (Ivison et al. 1991; Blair et al. 1983, and this paper) gives high values $[0.79 < E(B-V) < 1.4]$.

In the case of our analysis (Section 3.6), taking $T_{\rm e} = 10^5$ K, as we suggest in Section 3.5, would have reduced the value of $E(B-V)$ by approximately 0.6 across the image. Extinction determined from the hydrogen lines (as in Ivison et al. 1991; Blair et al. 1983) would be similarly affected by the assumed $T_{\rm e}$. In Paper I we presented evidence that the bipolar radio jets in CH Cyg included a non-thermal synchrotron emission component, where the relativistic electrons were accelerated through shock interaction and required the continuous injection of fresh electrons. In this case F_ν will be an overestimate of the true thermal contribution at 4.74 GHz, and so $E(B-V)$ will also be overestimated.

Conversely, if we take the ultraviolet-derived value of $E(B-V) \simeq 0.05$ as the true interstellar extinction, then a gas temperature of $\sim 10^5$ K is insufficient to fully explain the excess $E(B-V)$ determined from comparing the F487N image and the radio image. This means that there must be an additional contribution to the radio flux density over and above the thermal emission, further supporting the presence of a non-thermal component. We also note that the 2200-Å feature has not been seen in circumstellar dust, so that the ultraviolet (UV) method underestimates the total extinction in dusty sources.

An additional highly important effect influencing the extinction determination is that of self-absorption. This affects Hβ more strongly than Hα, and leaves the radio emission unchanged. Consequently, self-absorption has qualitatively the same effect as extinction by dust. If we consider the difference between the theoretical Hβ to Hα ratio and the observed ratio, this can account for an overestimate of perhaps 0.6 in $E(B-V)$, assuming that self-absorption is the only process causing this difference. From this it is clear that the combination of self-absorption, shock heating of the ejecta and a possible non-thermal radio component means that the value of $E(B-V)$ derived here can be readily reconciled with the much lower values derived for the field around CH Cyg and towards CH Cyg from fitting to the 2200-Å interstellar feature.

Table 3. Previous estimates of $E(B-V)$.

Date	$E(B-V)$ (mag)	Reference	Method
1988 September	0.79	1	Hα/Hβ
1980 August	1.05	2	Hα/Hβ
1985 May	0.1	3	2200 Å
1978	0.05	4	2200 Å
1985 January	0.01	5	2200 Å
1977 October to 1978 January 25	0.07	6	*BVRI*

References: 1 – Ivison et al. (1991); 2 – Blair et al. (1983); 3 – Mürset et al. 1991; 4 – Slovak (1982); 5 – Selvelli & Hack (1985); 6 – Slovak & Africano (1978).

4.4 Further *HST* images

Corradi et al. (2001) present a *HST* STIS CCD F28X50 O II image made on 1999 October 1, (dominated by the [O II] 3726-Å line). This image shows a number of arcs out to $\sim$4 arcsec from the central stars. We also note a northern feature which is symmetrically positioned about the central stars with the southern arcs; this feature is not commented upon by Corradi et al. (2001). Further knots and plumes at around 10 arcsec from the central stars are also seen in NOT images (see fig. 1 of Corradi et al.). The detail of the inner 2 arcsec of [O II] emission shows a southern extension coincident with the western edge of southern feature in e.g. Fig. 4(c). We therefore identify the southern extension in Fig. 4(c) as the inner arc, while referring to the main southern feature at $\sim$4 arcsec from the central stars as the outer arc.

We suggest three possible relationships between these arcs and the activity associated with the central stars.

(i) The southern arcs at both $\sim$1.7 and $\sim$4 arcsec are due to multiple ejection events closely spaced in time, and associated with a single active phase. This would obviously require the outer arc to be travelling at approximately twice the velocity of the inner arc, assuming a common origin at the central stars.

(ii) The southern arcs at $\sim$1.7 and $\sim$4 arcsec are due to separate ejection events widely spaced in time, possibly related to activity in the central binary (see further discussion in Section 4.5. If the velocities are comparable, then the outer arc will have been travelling perhaps 2–2.5 times as long as the inner arc, assuming a common origin at the central stars.

(iii) One or both of the southern arcs are structures in the winds of the giant components. In this case, the radio emission and other structures represent an interaction between outflow during the active phase and the existing giant winds.

4.5 The origin of the nebula

The H-line spectra from 1998 show a broad emission feature underlying the bright double-peaked features. This is consistent with the presence of a high-velocity wind. This feature forms at the beginning of the 1998 brightening, and so can be associated with the active star. Assuming this wind started close to the active star around

1998 September and expanded at a velocity of 1200 km s^{-1}, then by the time of the *HST* observations in 1999 August (∼340 days) we find that this wind should have an extent of 470 au. At the distance of CH Cyg, this is an angular size of ∼1.8 arcsec, comparable with that of the nebulosity seen in Figs 4 and 5. This is consistent with the idea that the inner nebulosity is ejected material associated with the optical active phases. It was noted in Paper I that the radio emission was typically significantly more extended during or shortly after previous active phases than during quiescent phases. The bipolar nature of the nebula in both 1999 and in earlier phases of extended emission (Taylor et al. 1986) is consistent with collimation of such an outflow either by an accretion disc or the giant winds.

Referring to Fig. 13, we can see that the different values of $R_{\rm O\,III}$ for the discrete features N, S1 and S2 allow a range of different conditions. The most difficult to understand are the diagnostic results for feature N. The $R_{\rm O\,III}$ locus does not intercept the $T_{\rm b}$ locus for the most likely value of $l = 70$ au. The largest value for which the $T_{\rm b}$ locus intercepts the $R_{\rm O\,III}$ locus is $l = 6.8$ au. In this case, $T_{\rm b} \simeq 2 \times 10^5$ K, $n_{\rm e} \simeq 10^6$ cm^{-3}, i.e. a dense, hot region which is physically thin along the line of sight. A more likely explanation is that the $R_{\rm O\,III}$ diagnostic is in some way contaminated for feature N. Such contamination could result from the star subtraction or an asymmetric continuum distribution, but it is difficult to assess the real cause.

The diagnostics for S1 and S2 are apparently more straight forward to describe. For the most likely value of $l = 70$ au, S1 has $T_{\rm b} \simeq 4.8 \times 10^4$ K, $n_{\rm e} \simeq 3 \times 10^5$ cm^{-3}. For $l = 35$ au, S2 has two points of intercept: $T_{\rm b} \simeq 4.4 \times 10^5$ K, $n_{\rm e} \simeq 2.2 \times 10^5$ cm^{-3}, and $T_{\rm b} \simeq 6 \times 10^6$ K, $n_{\rm e} \simeq 2.6 \times 10^5$ cm^{-3}. The largest value of l for a single intercept with the $R_{\rm O\,III}$ locus for S2 is 65 au, where $T_{\rm b} \simeq 1.6 \times 10^6$ K, $n_{\rm e} \simeq 2.3 \times 10^5$ cm^{-3}. These are clearly subject to some of the same sources of contamination as evidently affects $R_{\rm O\,III}$ for N, although presumably both the continuum and star subtraction have much lesser effects around S2.

In all cases it appears that $T_{\rm e} > 10\,000$ K, the canonical value for photoionized nebulae, and possibly $T_{\rm e} \gg 10\,000$ K. The only way the nebulosity could have a temperature $T_{\rm e} \sim 10\,000$ K is if $R_{\rm O\,III} \geqslant 30$, which seems an unlikely level of contamination. In addition, in Paper I we suggested that there was a non-thermal component to the extended radio emission. This would mean that the $T_{\rm b}$ loci appear at too large values of $n_{\rm e}$ (because $T_{\rm b}$ is overestimated), and require even greater values of $R_{\rm O\,III}$ to bring the $T_{\rm e}$ down to canonical photoionized values. These high electron temperatures can only be sustained if the outflowing material is shock heated, presumably by interaction with the pre-existing giant winds.

We suggest that nebula features seen in fig. 1 of Corradi et al. (2001) and Figs 4, 5 and 12 in this paper are due to ejecta associated with the 1998–2000 active phase. We see two arcs to the south, and possibly a third arc to the north, which we attribute to two closely timed ejection events around the 1998 brightening phase. The outer southern arc is due to a much more energetic event, and is consequently much more extended and less dense during our observations in 1999 October. A strong second possibility is that the outer arc originated with the 1992–1995 activity phase, again as ejecta. The ratio of the sizes of the arcs is comparable with the ratio of the times since activity started in each case, indicating two phases of ejecta expanding at similar projected velocities in the plane of the sky (∼1000 km s^{-1}). Corradi et al. (2001) report a tentative detection in N II of a third arc 0.35 arcsec to the west of the central stars. Again the ratios of the extents of these three arcs is in agreement with the time-separation of the three active phases, including the one that started in 1977. In this case, the expansion velocity in the plane of the sky would only be $\sim 260 \pm 50$ km s^{-1}. A third possibility is that the outer southern feature is a pre-existing structure in the winds of the giant components (travelling at a few 10s of km s^{-1}) which has been illuminated by the activity of the central star, and perhaps the action of associated ejecta. In any case, however, the inner features appear most consistent with directly imaged ejecta from the 1998–2000 active phase, explaining both the structure on the sky and the structure of emission lines from the spectra.

With imaging at further epochs, it should be possible to distinguish between these possibilities. We note for example that tracking of any motion of the outer southern arcs in particular will possible from ground-based studies and should therefore be attempted (Corradi et al. 1999, began this process). Ideally however further *HST* observations should be secured to answer these questions in a timely manner.

5 CONCLUSIONS

The results of this work include the following.

(i) Photometric observations show that during 1998 from May to July the brightness of CH Cygni increased by about 3 mag in U, entering a new active phase. Our observations also suggest the eclipse of the active star in the symbiotic pair by the giant in the outer orbit. The position, broadening and colours, of the dip, the disappearance of flickering in the blue continuum and the spectroscopic observations made during the minimum all suggest its eclipsing nature. From our long-term monitoring, we also suggest that the 1992–1995 and the 1998–2000 active phases began at the same orbital phase for the inner binary, $\sim 0.15 P_{\rm orb}$ before periastron passage.

(ii) Two types of mass outflow from the active star were observed: a high-velocity hot star wind plus a massive outflow indicated through a sporadic and complex absorption/emission structure of the P-Cygni type on the blue side of the hydrogen lines. The former is consistent with an outburst in the central part of the accretion disc around the active star, while the latter remains to be understood.

(iii) The timing and velocity of the fast wind seen prior to the eclipse would lead directly to a nebulosity of the extent seen in the *HST* and VLA images. At the same time, this wind develops when the hot star becomes active, and the loss of the feature in eclipse demonstrates that it is associated with the inner binary. Thus we have the first direct evidence linking the extended nebulosity to the fast wind generated when the hot star becomes active. In addition, more extended nebulosity could be due to either a second, more energetic ejection event in 1998, or an ejection event in 1992–1993 with similar velocity.

(iv) Comparison of the radio emission with the [O III] line ratio shows that the extended emission has electron temperatures ∼100 000 K, consistent with a shocked outflow. If the radio emission has a dominant non-thermal component, as suggested in Paper I, then this analysis is valid only for the thermal component of the electron population. However the magnetic field compression necessary for non-thermal emission also requires a shocked outflow. Thus, whatever the nature of the radio emission in the extended nebula, we can conclude that a shocked outflow is present. We also demonstrate that the combined affects of self-absorption in Balmer lines, a non-thermal component to the radio emission and shock heating of the ejecta make estimating $E(B-V)$ from *HST* and radio data impossible in the case of CH Cyg.

(v) The double-arc structure apparent at ∼4 arcsec and ∼1.8 arcsec from the star suggests that the ejection process is episodic. The smaller-scale arc is consistent with ejecta travelling

outwards at $\sim$1200 km s^{-1} following the brightening in 1998. This would place the outer arc either travelling much more rapidly and being ejected slightly earlier, or travelling at a similar velocity and hence being ejected a significant time before the 1998 brightening, perhaps during the 1992–1995 active phase. The latter explanation is consistent with the apparent lack of a higher velocity feature in the spectra. Alternatively one or both the arcs may be due to existing structures within the giant stars' winds, which have become apparent due to the impact of the activity in the central star and the development of high-velocity ejecta. Given the existence of wind features during the 1998–2000 activity, and the absence of such features outside of the active periods, we currently favour the explanation with multiple ejection events at different velocities.

ACKNOWLEDGMENTS

We thank the referee for helpful comments which have significantly strengthened this paper. We thank Faig Musaev for obtaining a spectrum at the Observatory on the peak Terskol. Thanks are also owed to Dr S. J. Smartt of the UK *HST* Support Unit for his essential assistance with the details of the imaging. We thank Dr R. L. M. Corradi for useful discussions. AS acknowledges the hospitality of the Astrophysics Research Institute of Liverpool John Moores University and the Astronomical Observatory di Capodimonte in Naples. The 1.82-m telescope at Mt. Ekar is operated by the Astronomical Observatory of Padova. This research was supported in part through Slovak Academy of Sciences grant No. 2/1157/01. SPSE was supported by a PPARC Research Assistantship for part of this work. The VLA is operated by the National Radio Astronomy Observatory, a facility of the National Science Foundation operated under co-operative agreement by Associated Universities, Inc.

REFERENCES

Anderson Ch. M., Oliversen N., Nordsieck K. H., 1980, ApJ, 242, 188
Biretta J., ed., 1996, WFPC2 Instrument Handbook, Version 4.0. STScI, Baltimore, MD
Blair W. P., Feibelman W. A., Michalitsianos A. G., Stencel R. E., 1983, ApJS, 53, 573
Bode M. F., Roberts J. A., Ivison R. J., Meaburn J., Skopal A., 1991, MNRAS, 253, 808
Cassatella A., Fernández–Castro T., González–Riestra R., Fuensalida J. J., 1992, A&A, 258, 368
Corradi R. L. M., Schwarz H. E., 1997, in Mikołajewska, J., ed., Physical Processes in Symbiotic Binaries. Copernicus Founation for Polish Astronomy, Warsaw, p. 147
Corradi R. L. M., Brandi E., Ferrer O. E., Schwarz H. E., 1999, A&A, 343, 841
Corradi R. L. M., Munari U., Livio M., Mampaso A., Goncalves D. R., Schwarz H. E., 2001, ApJ, 560, 912
Crocker M. M., Davis R. J., Eyres S. P. S., Bode M. F., Taylor A. R., Skopal A., Kenny H. T., 2001, MNRAS, 326, 781 (Paper I)
Deutsch A. J., 1964, Ann. Rep. Mt. Wilson and Palomar Obs., 11
Eyres S. P. S., Bode M. F., Taylor A. R., Crocker M. M., Davis R. J., 2001, ApJ, 551, 512
Hack M., Engin S., Rusconi L., Sedmak G., Yilmaz N., Boehm C., 1988, A&AS, 72, 391
Henden A. A., Kaitchuck R. H., 1982, Astronomical Photometry. Van Nostrand Reinhold Company, New York, p. 50
Hinkle K. H., Fekel F. C., Johnson D. S., Scharlach W. W. G., 1993, AJ, 105, 1074
Iijima T., 1998, MNRAS, 297, 77
Ivison R. J., Bode M. F., Roberts J. A., Meaburn J., Davis R. J., Nelson R. F., Spencer R. E., 1991, MNRAS, 249, 374
Kenyon S. J., 1986, The Symbiotic Stars. Cambridge Univ. Press, Cambridge
Mikkola S., Tanikawa K., 1998, AJ, 116, 444
Mikołajewska J., 1997, Physical Processes in Symbiotic Binaries and Related Systems. Fundacja Astronomii Polskiej im. Mikołaja Kopernika, Warsaw
Mikołajewski M., Tomov T., 1986, MNRAS, 219, 13
Mikołajewski M., Mikołajewska J., Tomov T., 1987, Ap&SS, 131, 733
Mikołajewski M., Mikołajewska J., Khudyakova T. N., 1990, A&A, 235, 219
Musaev F. A., 1998, Sov. Astron. Lett., 19, 776
Mürset U., Nussbaumer H., Schmid H. M., Vogel M., 1991, A&A, 248, 458
Osterbrock D. E., 1989, Astrophysics of Gaseous Nebulae and Active Galactic Nuclei. University Science Books, Mill Valley CA
Panchuk V. E., 1998, The Main Stellar Spectrograph of the 6-m Telescope. SAO Technical Report No. 258 (in Russian)
Reiss A., 2000, WFPC2 Instrument Science Report 00–04. STScI, Baltimore
Robinson K., Bode M. F., Skopal A., Ivison R. J., Meaburn J., 1994, MNRAS, 269, 1
Selvelli P. L., Hack M., 1985, Astronomy Express, 1, 115
Sion E. M., 1997, in Mikołajewska J., ed., Physical Processes in Symbiotic Binaries. Copernicus Founation for Polish Astronomy, Warsaw, p. 49
Skopal A., 1995, IBVS No. 4157
Skopal A., 1997, in Mikołajewska J., ed., Physical Processes in Symbiotic Binaries. Copernicus Founation for Polish Astronomy, Warsaw, p. 99
Skopal A., Mikołajewski M., Biernikowitz R., 1989, Bull. Astron. Inst. Czechosl., 40, 333
Skopal A., Bode M. F., Lloyd H. M., Tamura S., 1996a, A&A, 308, L9
Skopal A. et al., 1996b, MNRAS, 282, 327
Skopal A., Vittone A., Errico L., Bode M. F., Lloyd H. M., Tamura S., 1997, MNRAS, 292, 703
Skopal A., Bode M. F., Lloyd H. M., Drechsel H., 1998a, A&A, 331, 179
Skopal A., Bode M. F., Lloyd H. M., Drechsel H., 1998b, A&A, 331, 224
Slovak M. H., 1982, in NASA, Goddard Space Flight Center Advances in Ultraviolet Astronomy. N82-31163 21-89, p. 448
Slovak M. H., Africano J., 1978, MNRAS, 185, 591
Taylor A. R., Seaquist E. R., Mattei J., 1986, Nat, 319, 38
Viotti R., Badiali M., Cardini D., Emanuele A., Iijima T., 1997, in Battrick B., ed., Hipparcos – Venice 1997, ESA SP–402. ESA Publ. Div., Noordwijk, p. 405
Whitmore B., 1998, Technical Instrument Report WFPC2 98–01. STScI, Baltimore, MD
Whitmore B., Heyer I., 1998, Instrument Science Report WFPC2 97–08. STScI, Baltimore, MD

This paper has been typeset from a TEX/LATEX file prepared by the author.